Supplementary Information

Spray-Combustion Synthesis. Efficient Solution Route to High-Performance Oxide Transistors

Xinge Yu,[a,b] Jeremy Smith,[a] Nanjia Zhou,[c] Li Zeng,[d] Peijun Guo,[c] Yu Xia,[e] Ana Alvarez,[e] Stefano Aghion,[f] Hui Lin,[a,b] Junsheng Yu,[b] Robert P. H. Chang,*[c] Michael J. Bedzyk,*[c] Rafael Ferragut*[f], Tobin J. Marks*[a,c], Antonio Facchetti*[a,e]

[a]Department of Chemistry and the Materials Research Center, Northwestern University 2145 Sheridan Road, Evanston, Illinois, 60208 (USA)

[b]State Key Laboratory of Electronic Thin Films and Integrated Devices, School of Optoelectronic Information, University of Electronic Science and Technology of China (UESTC), Chengdu, 610054 (China)

[c]Department of Materials Science and Engineering and the Materials Research Center, Northwestern University, 2220 Campus Dr., Evanston, Illinois, 60208 (USA)

[d]Applied Physics Program and the Materials Research Center, Northwestern University, 2220 Campus Dr., Evanston, Illinois, 60208 (USA)

[e]Polyera Corporation, 8045 Lamon Avenue, Skokie, Illinois, 60077 (USA)

[f]LNESS and CNISM, Dipartimento di Fisica, Politecnico di Milano, Via Anzani 42, Como, 22100 (Italy), Istituto Nazionale di Fisica Nucleare, via Celoria 16, Milano, 20133 (Italy)

E-mail: bedzyk@northwestern.edu; rafael.ferragut@polimi.it ; t-marks@northwestern.edu ; a-facchetti@northwestern.edu

X. Y. and H. L. are on leave from University of Electronic Science and Technology of China

Keywords: thin film transistor (TFT), solution process, metal oxide, combustion synthesis, spray-coating

Experimental Section

Metal Oxide film and transistor fabrication. Doped Si/SiO_2 wafers (300 nm, C_i = 10.5nF cm^{-2} WRS Materials; solvent cleaned, then cleaned with an O_2 plasma for 5min) were used as the gate electrode/dielectric layer. For the other MO dielectrics, amorphous Al_2O_3 (C_i = 160nF cm^{-2}) and ZrO_2 (C_i = 255nF cm^{-2}) dielectric films were grown on the appropriate substrates as reported previously (see SI). In_2O_3, IZO, and IGZO films were deposited by SCS, spin-SC, sol-gel, all in a well-ventilated fume hood, or magnetron-sputtering as indicated below. Finally, 40nm Al source/drain electrodes (W/L = 1000μm/50μm) were evaporated through a shadow mask.

Precursor solutions for SCS and spin-CS. All reagents were used as received from Sigma-Aldrich. These solutions were prepared with $In(NO_3)_3 \cdot xH_2O$, $Zn(NO_3)_2 \cdot xH_2O$, and $Ga(NO_3)_3 \cdot xH_2O$ in 2-methoxyethanol to yield 0.05 or 0.5 M solutions. For 0.05 [or 0.5] M solutions, 55 [or 110] μL NH_4OH and 100 [or 200] μL acetylactone were added to 10 [or 2] mL of the metal solutions and stirred overnight at 25°C. Prior to spin- or spray-coating, the precursor solutions were combined in the desired molar ratios and stirred for 2h. All depositions were carried out at RH<30%.

<u>SCS</u>: Substrates were maintained at 200-350 °C on a hot plate while 0.05M precursor solutions were loaded into the spray gun and sprayed intermittently (60s cycles) on the substrates until the desired thickness (20, 50nm) was obtained. The drop feature size is between 30 to 150 μm, depending on the processing temperature. The nozzle-substrate distance was 10-30cm.

<u>Spin-CS</u>: For 20nm thick (4 layers) devices, 0.05M precursor solutions were spin-coated at 3500rpm for 30s, and then annealed for 30min at 200-350°C; this was repeated 4x to achieve the desired thickness. For one-step 50nm single layer devices, precursor solutions with concentrations of 0.5M were spin-coated at 2000rpm for 60s, and then annealed for 30min at the desired temperature.

<u>Spray:</u> The precursor solution and coating process was identical to that of SCS but without acetylacetone.

<u>Sol-gel</u>: These solutions were prepared with $In(NO_3)_3 \cdot xH_2O$, $Zn(NO_3)_2 \cdot xH_2O$, and $Ga(NO_3)_3 \cdot xH_2O$

in 2-methoxyethanol with a concentration of 0.5M, and then stirred overnight at 25°C. Prior to spin- coating, the precursor solutions were combined in the desired molar ratios and stirred for 2h. For one-step 50nm single layer films, the precursor solutions were spin-coated at 2000 rpm for 60s, and then annealed for 30min at the desired temperature.

Sputtering: 50nm IGZO films were sputtered (1:1:1 target from Nikko Denko) using magnetron- sputtering equipment (AIA International) with a base pressure $<10^{-5}$Torr and a Ar/O_2 mixture (20 sccm:1 sccm). After sputtering, the films were annealed at 350°C for 60 min.

Al_2O_3 and ZrO_x dielectric fabrication. Amorphous Al_2O_3 and ZrO_x dielectric films were grown using a procedure reported previously: $Al(NO_3)_3 \cdot xH_2O$, $ZrCl_4$ and $Zr(OCH(CH_3)_2)_4(CH_3)_2CHOH$ were used as the precursor for Al_2O_3 and ZrO_2, respectively.[1,2]

Oxide film morphology characterization. AFM film morphologies were imaged with a Veeco Dimension Icon scanning Probe Microscope using tapping mode. SEM images were recorded using a Hitachi S4800-II. XRD measurements were performed with a Rigaku ATX-G Thin Film Diffraction Workstation using Cu kα radiation coupled to a multilayer mirror. For STEM and TEM measurements, samples were prepared using both spin-coating (3500 rpm for 30 s, then annealing for 30 min, repeated four times) and spray-coating (see *Spray coating* section below) with 0.05 M precursor solution on NaCl substrates with either post annealing or situ annealing. The prepared sample was then lifted with an OmniProbe nanomanipulator and transferred to a semi-spherical Cu TEM grid. STEM imaging was conducted with a JEOL-2300F microscope, and TEM imaging was conducted with a JEOL-2100F microscope. XPS (Omicron ESCA Probe) characterization of In 3d, Ga 3d, Zn 2p, and O 1s signals were monitored on metal oxide/SiO_2 after surface cleaning.

Electrical measurements. TFT device characterization was performed on a customized probe station in air with a Keithly 6430 subfemtometer and a Keithly 2400 source meter, operated by a locally written Labview program and GPIB communication. For bias stress and ultra-low current measurements a Keithley 4200 multi-channel electrometer was used. Four-probe conductivity measurements were carried out using an Agilent electrometer.

X-ray reflectivity measurements. XRR of the four IGZO film samples were performed on the 18 kW Rigaku ATXG workstation at the J.B. Cohen X-ray lab at Northwestern University. Cu kα X-

rays (wavelength is $\lambda = 0.1541$ nm) were generated and collimated to produce a monochromated beam of dimensions 5.0mm×0.1mm and 2×10^8 photons/sec flux at the sample surface. The XRR data were modeled and fit by applying an Abeles matrix method used in the Motofit package to obtain the thickness, electron density, and interfacial roughness information of each layer.

Mass density calculation by XRR: The X-ray reflectivity $R\,(Q)$ as a function of momentum transfer modulus $Q = 4\pi \sin(2\theta/2)\,/\lambda$ can be modeled by

$$\frac{R(Q)}{R_F(Q)} = \left| \int \left(\frac{d\rho}{dz}\right) e^{iQz} dz \right|^2$$

where $R_F(Q)$ is the Fresnel reflectivity from an ideal substrate (Si) mirror surface , and $\rho(z)$ is the electron density profile along the surface normal normalized to the substrate density. XRR analysis determines the film electron density (ρ_e), film thickness, and interfacial/surface roughness. For a given composition, the mass density (ρ_m) can be calculated from

$$\rho_m = \frac{\rho_e}{N_e} M \frac{1}{N_A}$$

where *M* is molar mass, N_e the total film electron number, and N_A is Avogadro's constant.

Positron annihilation spectroscopy. PAS was used to monitor the porosity of some selected IGZO films. In order to obtain depth-resolved data, positrons were implanted in the sample at various depths using a variable-energy positron beam at the *VEPAS* laboratory (LNESS Centre - Politecnico di Milano). The depth resolution of a variable-energy positron beam depends on the positron implantation-profiles of the so-called Makhov distribution, that is narrow at low positron implantation energy and broader at high implantation energy.[3] The explored region after implantation depends on the positron and positronium diffusion length. Positronium diffusion depends on the pore dimensions and the pick-off conversion.[3] A hyperpure Ge γ-ray detector was used to measure the spectrum of the annihilation radiation. This spectrum contains a peak centered at 511 keV, which comes from two-γ positron-electron annihilation, and a continuous distribution below 511 keV, coming from three-γ annihilation of positronium atoms formed at the open pores into the amorphous films. The two-γ peak, which is broadened by the Doppler effect due to the motion of the electrons encountered by positrons, bears the

signature of the chemistry and defectivity of the material. The *S*-parameter corresponds to annihilation of positrons with valence electrons and Ps annihilation (para-Ps and ortho-Ps pick-off that annihilate in two-γ rays). This parameter was taken in the energy range 511±0.85 keV. In the present work, the *S*-parameter was normalized to the Si bulk value ($S_r = S/S_{Si}$, with $S_{Si} \approx 0.54$). An additional PAS parameter, sensitive to the presence of free volume and to the extension of inner pore surface, is the positronium fraction. Ps fraction measurements were performed using the well-known "3γ method".[4] From the annihilation spectrum it is possible to obtain the *R(E)* parameter,

$$R(E) = \frac{V}{P}$$

where *P* and *V* are the integrated counts (after background subtraction) in the peak (511±4.25 keV) and valley area above the Compton edge, from 350 keV up to 500 keV, of the energy γ spectrum. When there is no pick-off annihilation, i.e., when the positronium is emitted in vacuum, the Ps fraction *F(E)* can be obtained from *R(E)* using the relationship:

$$F(E) = \left[1 + \frac{P_1(R_1 - R(E))}{P_0(R(E) - R_0)} \right]^{-1}$$

where P_0 and R_0 are the parameters when the Ps fraction is nil (*F*=0) and P_1 and R_1 are the parameters when 100% of the positrons becomes positronium (*F*=1). The calibration for 0% and ~100% of Ps in vacuum was performed using a Ge single crystal (100) at 1000 K.

The PAS results ($F_{3\gamma}$ and S_r parameters), as mentioned in the text, confirm that the SCS 1:0.1:0.29 and sputtered 1:1:1 films are the most compact. For a quantitative estimation, a fitting procedure represented by the continuous curves through the experimental points of the S_r evolutions in Figure S17 (VEPFIT[5]) was implemented. This software is a best fit procedure based on the solution of the diffusion equation in each layer of a heterostructure, taking into account the positron implantation-profiles dependent on energy.[6] The mean positron implantation depth Z_m depends on the positron implantation energy *E* according to the formula,

$$Z_m = \frac{A}{\rho} E^n$$

with n and A semi-empirical parameters (n= 1.6 and A= 40 nm g cm^{-3} keV$^{-1.6}$), ρ the mass density in g cm^{-3} and E in keV (this equation was used in Figure 4c for representing the PAS data as a function of the positron implantation depth). The fitting procedure is based on a model that schematically divides the explored regions in three layers: IGZO, SiO$_2$ and the silicon substrate, separated by three interfaces (vacuum/IGZO –surface–, IGZO/SiO$_2$ and SiO$_2$/Si). The interfaces were taken to be very thin ~1 nm and completely absorbing, i.e. inside of them the positron diffusion length is <1 nm.[7] The positron diffusion lengths L^+ in the IGZO films are about 11 nm (see Table S1) in both films, while the positronium diffusion lengths were 2(1) nm.

The thicknesses of the IGZO films were measured accurately by XRR with an absolute error of about 1 nm (see Table S1 and dashed line in Figure S17). Based on these thickness values, the mass densities of the films were estimated, minimizing the reduced chi-square statistics of the model fits χ^2_R. Figure S17 shows the χ^2_R plots where the obtained values that minimize the fits are: ρ_{sputt}= 5.8(2) g cm^{-3} and ρ_{SCS}= 6.4(2) g cm^{-3}. The IGZO films 1:1:1: spin-CS, sol-gel and SCS were also fit and the values of the number densities are: <5.2 g cm^{-3}, <5.4 g cm^{-3}, and 5.6 (2) g cm^{-3}, respectively. In the case of spin-CS and sol-gel films the S_r parameter is under the saturation regime (an important amount of positronium -- para-Ps and ortho-Ps pick-off -- annihilates to two-gamma rays in the amorphous films) and, in these cases, the obtained diffusion lengths in the films are highly influenced by Ps diffusion. For this reason the number densities in spin-CS and sol-gel films are considered upper limits. The porosities of the 1:1:1 films (sol-gel, combustion, SCS and sputtering) were estimated considering the density of a IGZO single crystal (ρ_{IGZO} ~6.2 g cm^{-3}):[6] $p_{sol-gel}$ >15%; p_{comb} >16%; p_{SCS}= 10(2)% and p_{sputt}= 6(2)%. By comparison between the PAS results between sputtered 1:1:1 and SCS 1:0.1:0.29, we conclude that the porosity of the latter indium-rich film is approximately the same as the sputtered film, i.e. ~6%.

In order to obtain an estimate of the mean cavity size and other useful parameters, two porous film families were considered:

- *The most porous films (sol-gel, spin-SC and SCS 1:1:1).* According to the XRR estimates the porosity p of the sol-gel and spin-SC films is about 40% (p= (1-ρ_m/ρ_{SC})= V_V/V_T= v_V, where ρ_m and ρ_{SC} are the mass densities measured in the film and of the single

6

crystals,[P6] respectively, V_V and V_T are the free and total volume, respectively, and v_V is the free volume per volume unit. This high porosity allows us to hypothesize a high degree of pore connectivity. In this condition, the Ps diffusion length is a good indication of the average pore size Φ,[P1] which is around 2.5(5) nm. On the other hand, an estimation of the cavity number density η let to verify the interconnectivity hypothesis. Considering that the porosity (or v_V) is equal to the number density of cavities multiplied by the unitary average free volume V_U ($v_V = \eta\ V_U = \eta\ {}^4/_3\ \pi\ (\Phi/2)^3$, where $V_U \sim 10$ nm^3 = 10^{-20} cm^3) η is equal to 4×10^{19} cm^{-3}. These values are within the condition of pore interconnection, i.e., according to the proposed approximation, it is frequent the superposition or packing of spheres of vacuum zones.

Following the same ideas 1:1:1 SCS has a porosity ~10%, a mean pore size 1.5(5) nm and a number density of cavities ~6×10^{19} cm^{-3} ($V_U \sim 1.8$ nm^3 = 1.8×10^{-21} cm^3). In this condition the porous connectivity is low.

- *The most compact films (sputtered 1:1:1 and SCS 1:0.1:0.29).* From the $F_{3\gamma}$ measurements it is possible to obtain an upper-limit of the pore dimension of ~1 nm (where $F_{3\gamma} \to 0$, see manuscript).[P5,P7] Besides, the minimum pore size in an amorphous film is about 4 Å (to be not considered as a vacancy or as a small vacancy cluster). The porosity of this films was estimated to be about 6% from PAS and XRR measurements. Thus, the number density is ~2×10^{20} cm^{-3} ($V_U \sim 0.3$ nm^3 = 3×10^{-22} cm^3, considering an average diameter of the cavity ~7-8 Å). In this case the possibility of pore interconnection is very low.

C–V measurements and trap density extraction. C–V measurements are made on MIS structures and with frequency kept low enough to monitor the trapping and detrapping mechanism. The MIS structure does not require frequencies as low as the TFTs because charges do not have to travel laterally from channel to the source/drain contacts. Therefore all measurements were made at 1 kHz. From the C–V data we can extract the surface potential, φ_s, (i.e., the potential at the semiconductor dielectric interface where $x = 0$). This comes from the surface charge accumulated, Q:

$$Q = C_i\left(V_G - \varphi_s\right)$$

Differentiating this w.r.t V_G and knowing that the measured capacitance, C, will be dQ/dV_G, then:

$$\frac{\partial \varphi_s}{\partial V_G} = 1 - \frac{1}{C_i}\frac{\partial Q}{\partial V_G} = 1 - \frac{C}{C_i}$$

Therefore we can find φ_s by integrating our capacitance normalized to the capacitance of the dielectric:

$$\varphi_s - \varphi_0 = \int_{V_{fb}}^{V_G}\left(1 - \frac{C}{C_i}\right)dV_G'$$

Note that this requires an estimate of the flat-band voltage V_{fb} which is taken as the point at which the C–V data starts to rise. This could be a significant source of error as the surface potential is very sensitive to V_{fb} and C_i. We can also find the surface potential gradient by applying Gauss's Law at the semiconductor-dielectric interface:

$$\varepsilon_s \left.\frac{\partial \varphi}{\partial x}\right|_{x=0} = \varepsilon_i \frac{(V_G - \varphi_s)}{t_i}$$

ε_s = semiconductor dielectric constant

ε_i = insulator dielectric constant

t_i = insulator thickness

These data provide the boundary conditions for solving Poisson's equation in the semiconductor. Poisson's equation, where n is the charge density, is:

$$\frac{\partial^2 \varphi(x)}{\partial x^2} = -q\frac{n(x)}{\varepsilon_s \varepsilon_0}$$

The charge density, n, consists of the free and trapped carriers:

$$n_{free} = n_i \exp\left(\frac{q\varphi(x)}{kT}\right)$$

$$n_{trap} = \int_0^{q\varphi(x)} D_{tr}(\varphi(x))dE$$

D_{tr} is the density of trap states. Therefore we are solving,

$$\varepsilon_s\varepsilon_0 \frac{\partial^2 \varphi(x)}{\partial x^2} + qn_i \exp\left(\frac{q\varphi(x)}{kT}\right) + q\int_0^{q\varphi(x)} D_{tr}(\varphi(x))dE = 0$$

to get the potential distribution, $\varphi(x)$, in the semiconductor for each gate voltage.

However, D_{tr} is unknown and is sought. It is also a function of the potential, therefore we must iterate over each gate voltage solving the Poisson equation and estimate values of D_{tr} to obtain

8

the correct surface potential and potential gradient from the *C–V* data. The boundary conditions for the Poisson equation are:

$$\varphi(0) = \varphi_s$$

$$\left.\frac{\partial \varphi}{\partial x}\right|_{x=t_s} = 0$$

The problem is that this is a non-linear second order partial differential equation and the solution can be unstable. It therefore requires small V_G steps and many iterations.
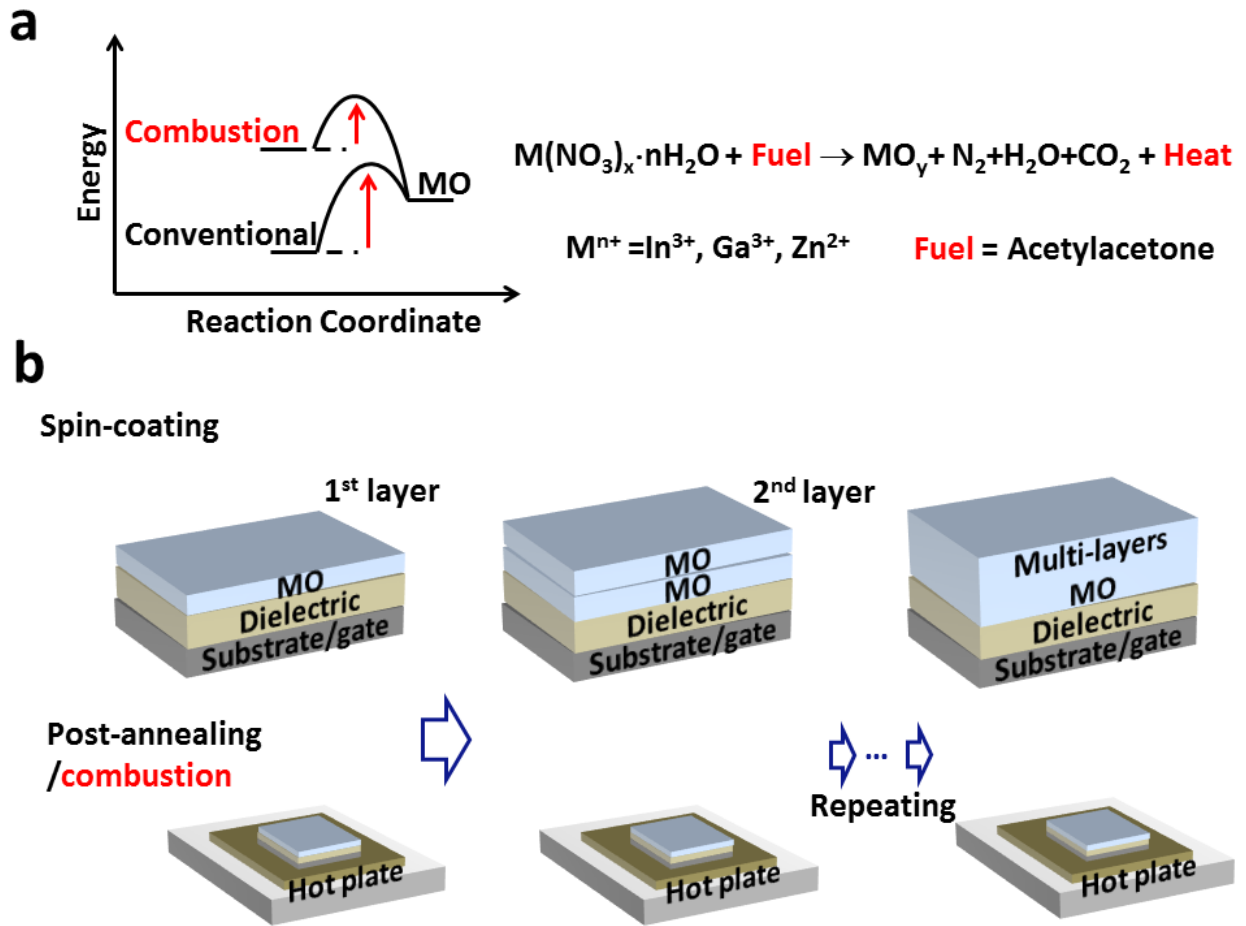
a

$$M(NO_3)_x \cdot nH_2O + \textbf{Fuel} \rightarrow MO_y + N_2 + H_2O + CO_2 + \textbf{Heat}$$

$$M^{n+} = In^{3+}, Ga^{3+}, Zn^{2+} \qquad \textbf{Fuel} = \text{Acetylacetone}$$

b

Figure S 1. **a**, Schematic reaction coordinate comparing the energetics of combustion synthesis and conventional sol-gel solution processing, and combustion reaction for a generic metal with nitrate acting as the oxidizer and acetylacetone as the fuel. **b**, Example of the conventional spin-coating/combustion process for metal oxide films deposition.
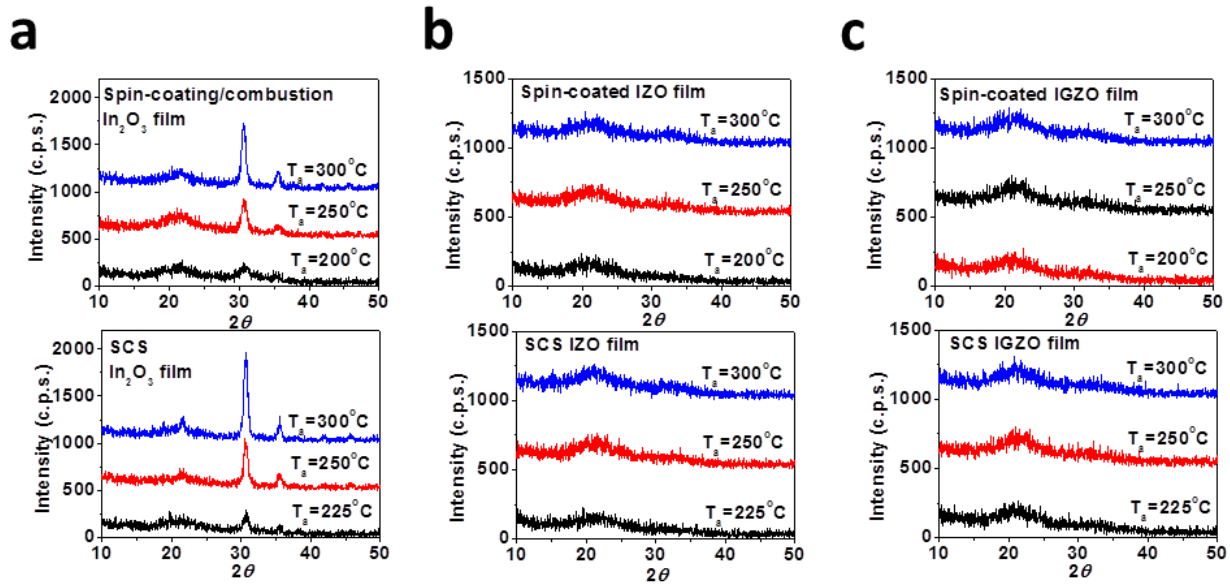
Figure S2. **a-c.** X-ray diffraction (XRD) patterns of various 20 nm thick oxide films for different combustion processing temperatures deposited using spin-coating and SCS. **a**, For In_2O_3 films. **b**, For IZO films. **c**, For IGZO films.
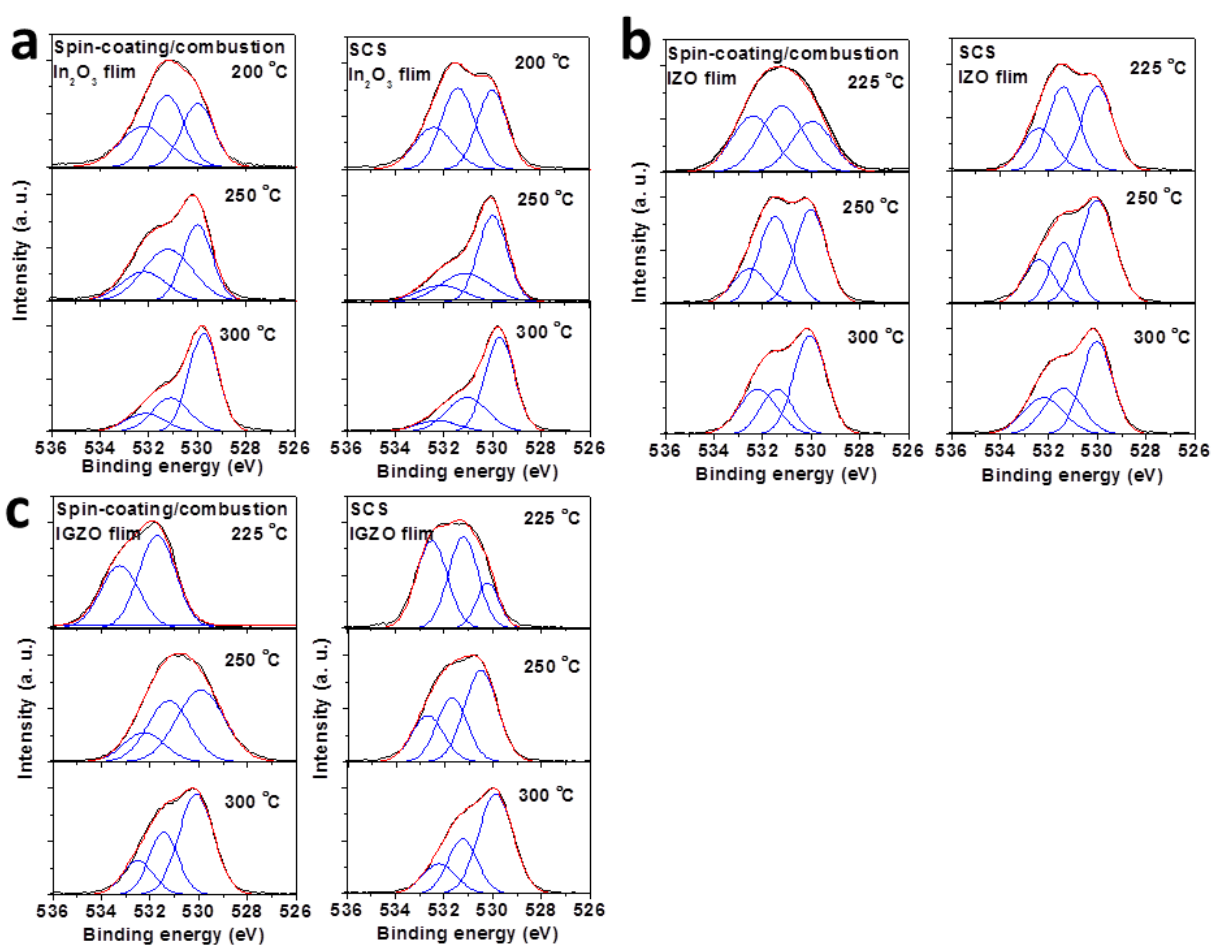
Figure S3. X-ray photoelectron spectra of 20 nm thick oxide films deposited at different processing temperatures. **a**, for In_2O_3. **b**, for IZO. **c**, for IGZO. 529.9± 0.1 eV: M-O-M lattice oxygen; 531.3 ±0.1 eV: M-OH metal hydroxide oxygen; 532.2 ± 0.1 eV: adsorbed oxygen species.
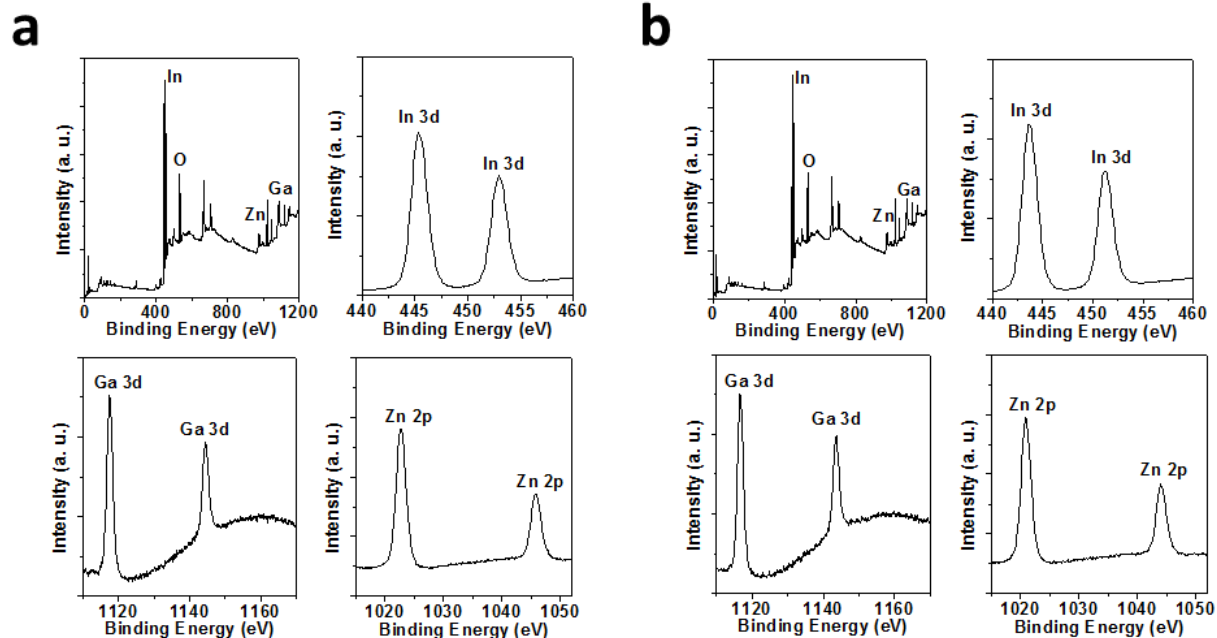
Figure S4. X-ray photoelectron spectroscopy (XPS) survey scans of the In 3d, Ga 3d, and Zn 2p peaks for combustion 20 nm thick IGZO films annealed at 300 °C: **a,** deposited by spin-coating, **b,** deposited by SCS.

a

T$_a$ = 200°C
RMS ~ 0.2 nm

T$_a$ = 225°C
RMS ~ 0.2 nm

T$_a$ = 250°C
RMS ~ 0.2 nm

T$_a$ = 300°C
RMS ~ 0.2 nm

b

T$_a$ = 225°C
RMS ~ 0.2 nm

T$_a$ = 250°C
RMS ~ 0.2 nm

T$_a$ = 300°C
RMS ~ 0.2 nm

c

T$_a$ = 225°C
RMS ~ 0.2 nm

T$_a$ = 250°C
RMS ~ 0.2 nm

T$_a$ = 300°C
RMS ~ 0.2 nm
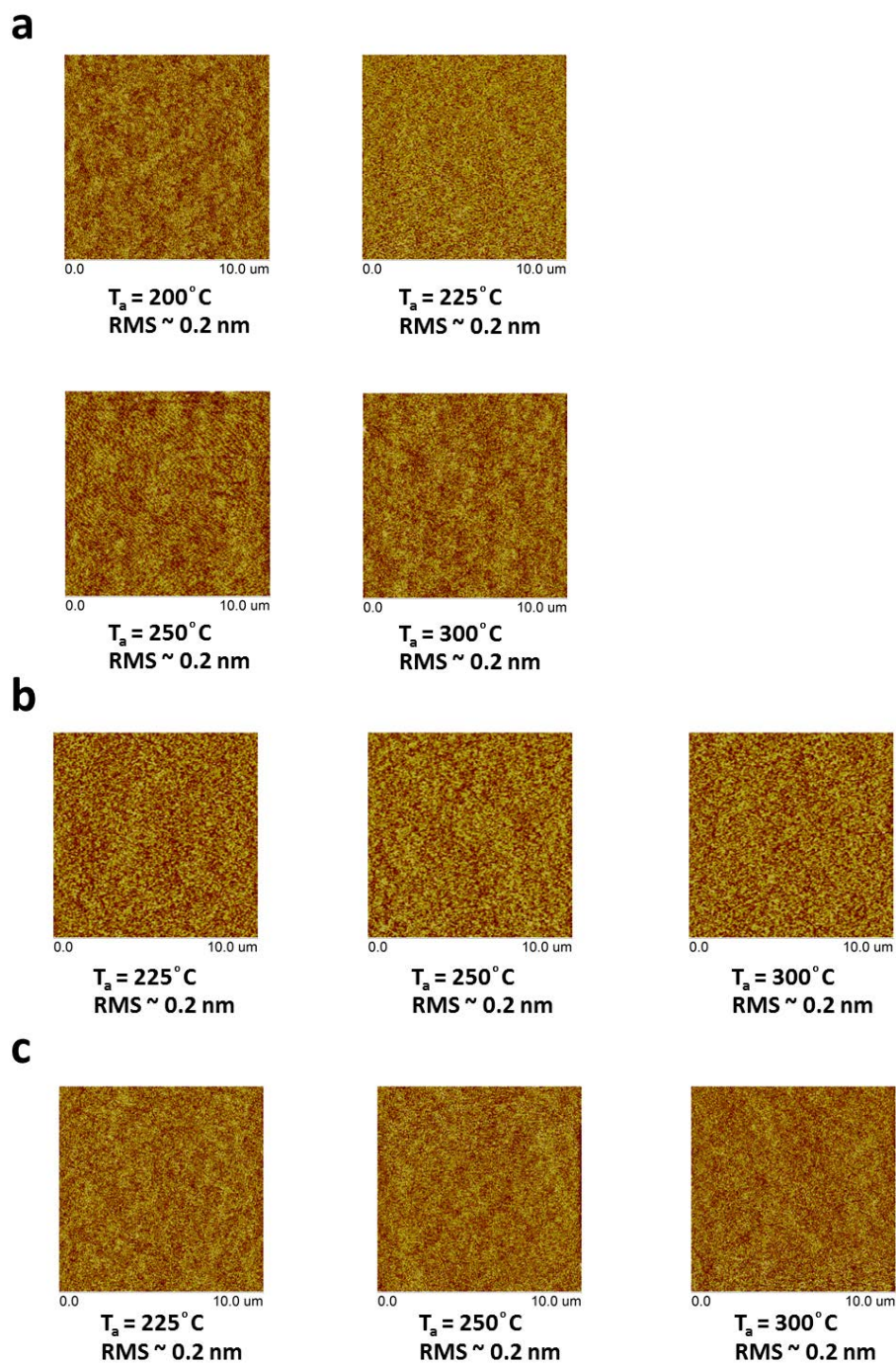
Figure S5. Atomic force microscopy (AFM) images of 20 nm thick spin-coated **a,** In$_2$O$_3$, **b,** IZO, and **c,** IGZO films on SiO$_2$ annealed at the indicated temperatures..

a

T$_a$ = 200°C
RMS ~ 0.6 nm

T$_a$ = 225°C
RMS ~ 0.5 nm

T$_a$ = 250°C
RMS ~ 0.5 nm

T$_a$ = 300°C
RMS = ~ 0.6 nm

b

T$_a$ = 225°C
RMS ~ 0.6 nm

T$_a$ = 250°C
RMS ~ 0.5 nm

T$_a$ = 300°C
RMS ~ 0.5 nm

c

T$_a$ = 225°C
RMS ~ 0.5 nm

T$_a$ = 250°C
RMS ~ 0.6 nm

T$_a$ = 300°C
RMS ~ 0.6 nm
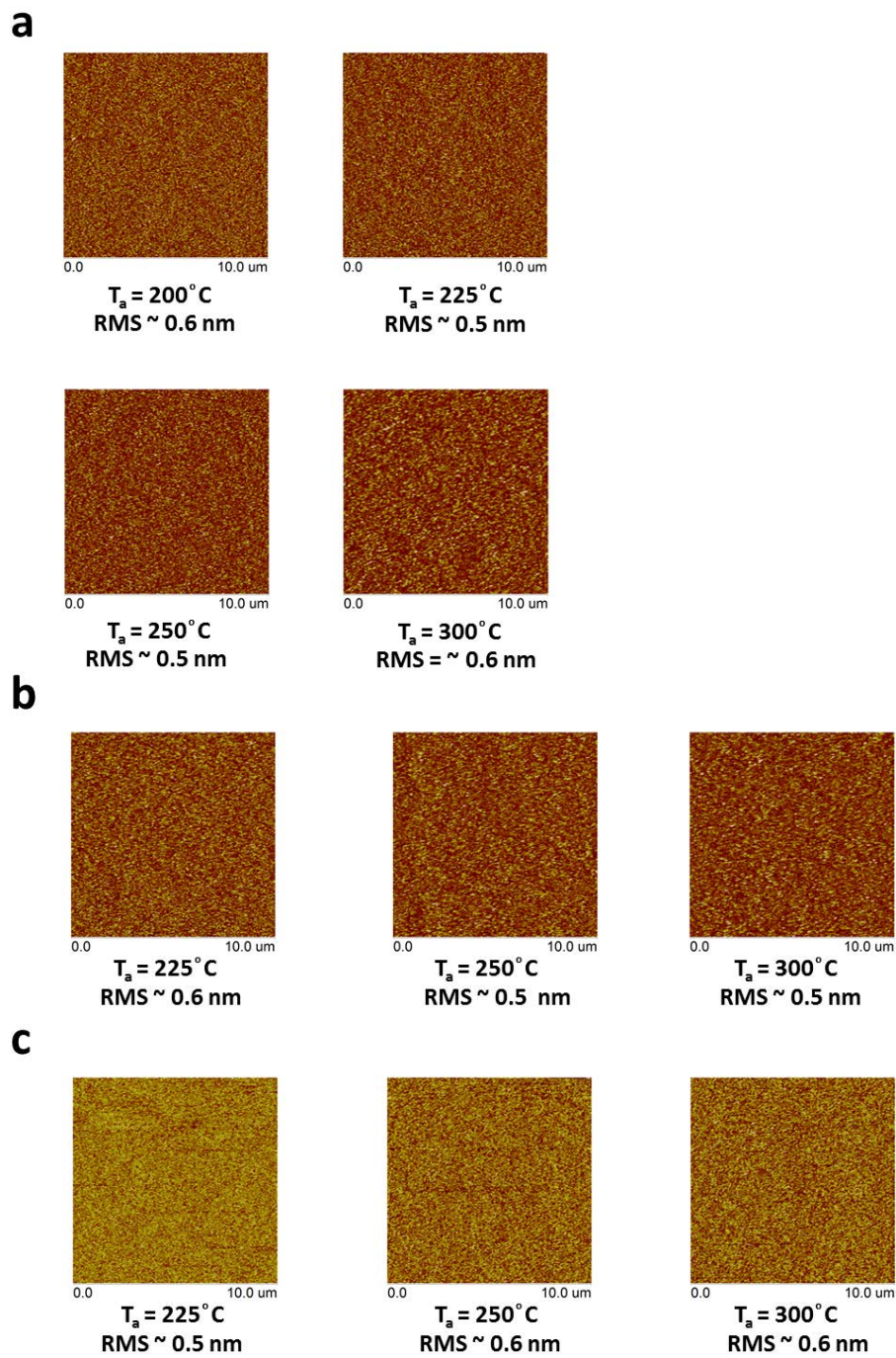
Figure S6. Atomic force microscopy (AFM) images of SCS 20 nm thick **a,** In$_2$O$_3$, **b,** IZO, and **c,** IGZO films on SiO$_2$ annealed at the indicated temperatures.

a
0.0   50.0 um
$T_a = 200°C$
RMS ~ 0.4 nm

b
0.0   10.0 um
$T_a = 200°C$
RMS ~ 0.5 nm

c
0.0   2.0 um
$T_a = 200°C$
RMS ~ 0.2 nm
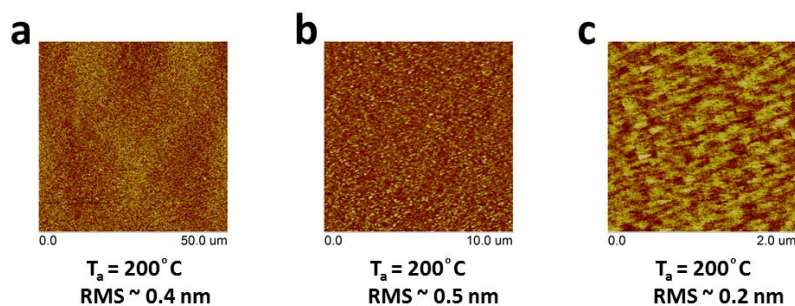
Figure S7. Atomic force microscopy (AFM) images of 20 nm SCS In_2O_3 films scanned over the indicated areas: **a,** 50 μm × 50 μm, **b,** 10 μm × 10 μm, and **c,** 2 μm × 2 μm.

a
0.0   10.0 um
In_2O_3
$T_a = 300°C$
RMS ~ 0.7 nm

b
0.0   10.0 um
IZO
$T_a = 300°C$
RMS ~ 0.7 nm

c
0.0   10.0 um
IGZO
$T_a = 300°C$
RMS ~ 0.7 nm
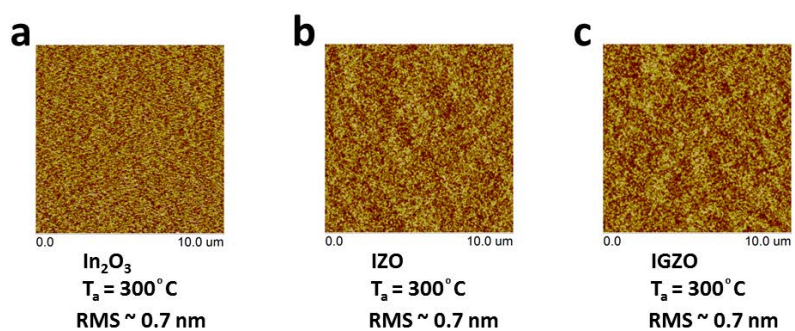
Figure S8. Atomic force microscopy (AFM) images of 50 nm SCS **a,** In_2O_3, **b,** IZO and **c,** IGZO films annealed at 300 °C
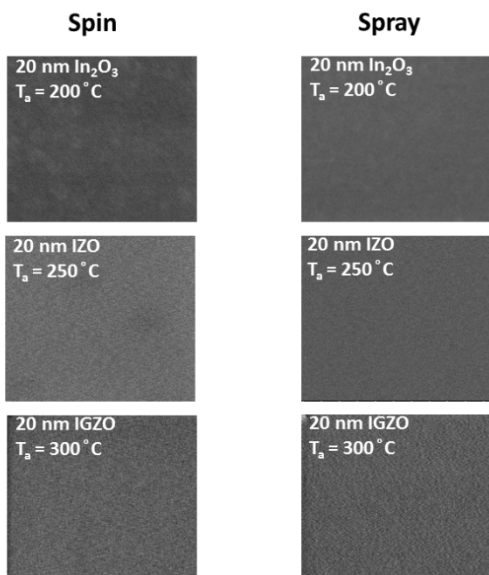
Figure S9. Scanning electron microscopy (SEM) images of 20 nm In_2O_3, IZO, and IGZO films deposited by spin-coating (5 nm ×4 layers) and SCS at the indicated processing temperatures
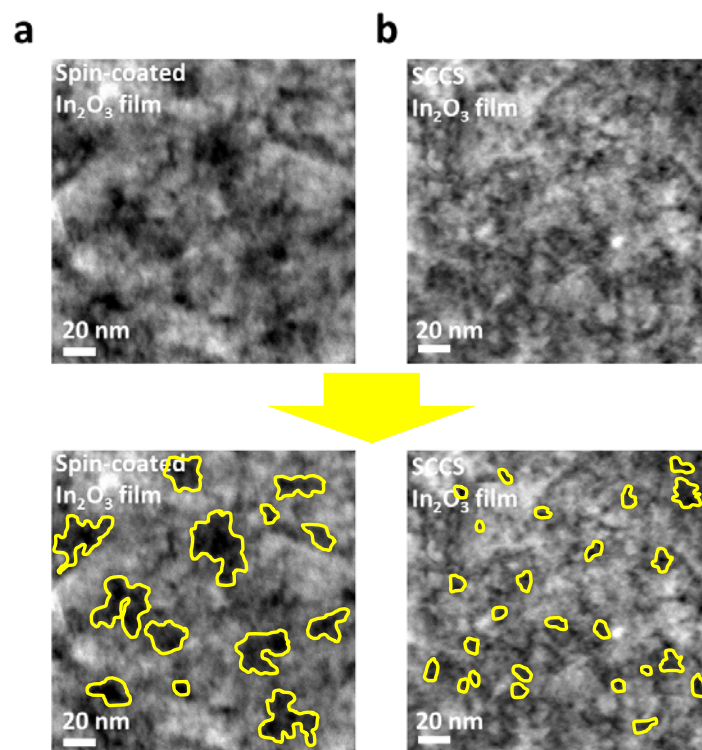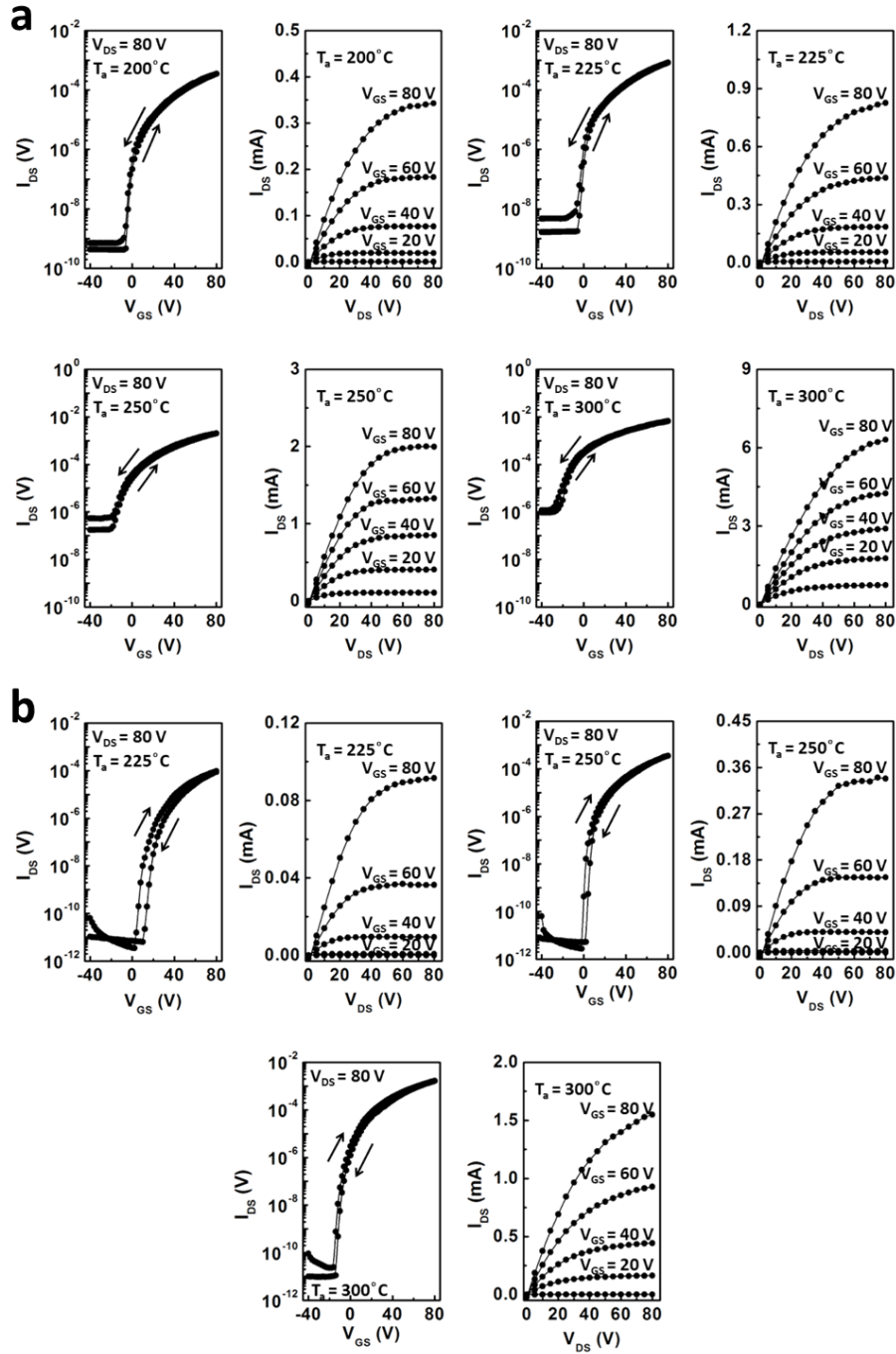
Figure S10. High angle annular dark field (HAADF) STEM images of In$_2$O$_3$ films deposited using **a.** spin-coating/combustion (5 nm$\times$ 4 layers), and **b.** deposited using SCS (20 nm) annealed at 300 °C.
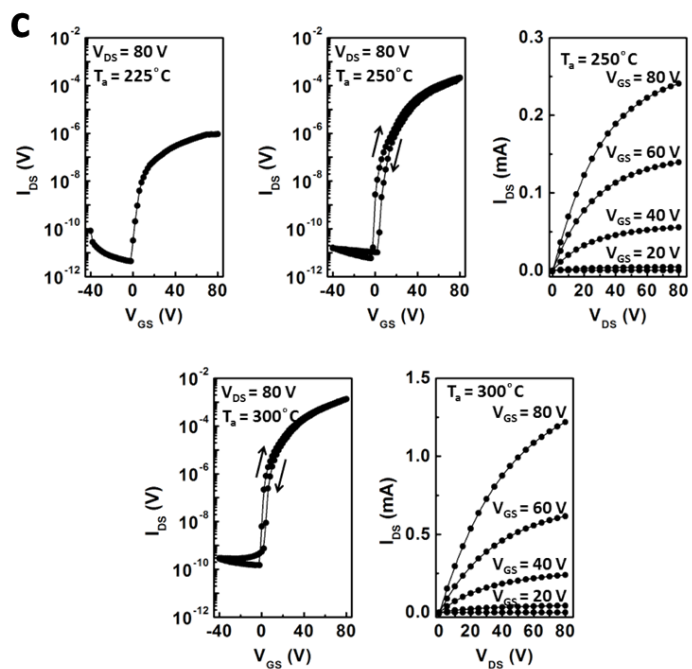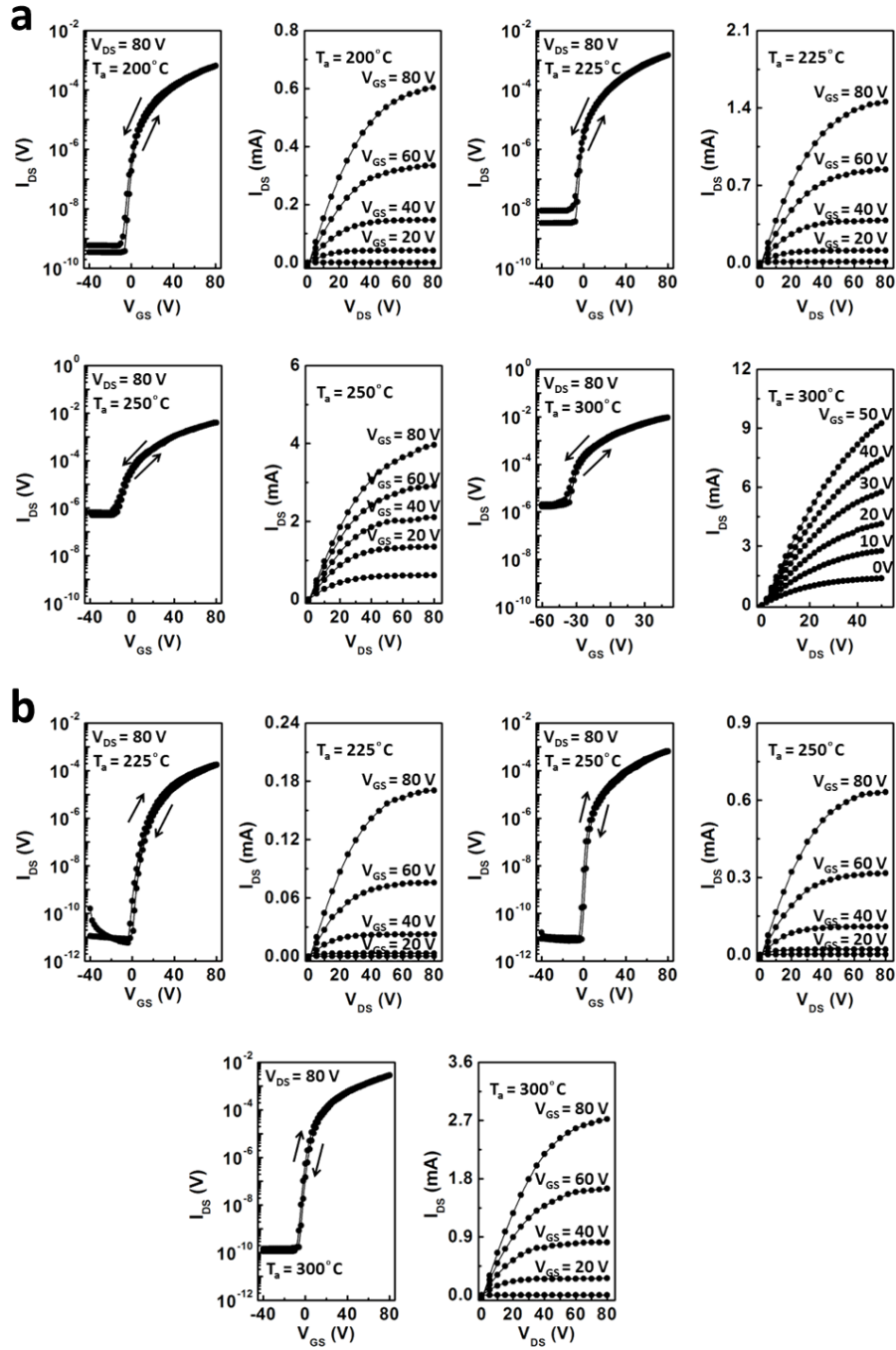
c

Figure S11. Transfer and output plots of the spin-coated 20 nm thick oxide films at various processing temperatures (on 300 nm SiO_2/Si substrates): **a,** In_2O_3 films, **b,** IZO films, **c,** IGZO films.
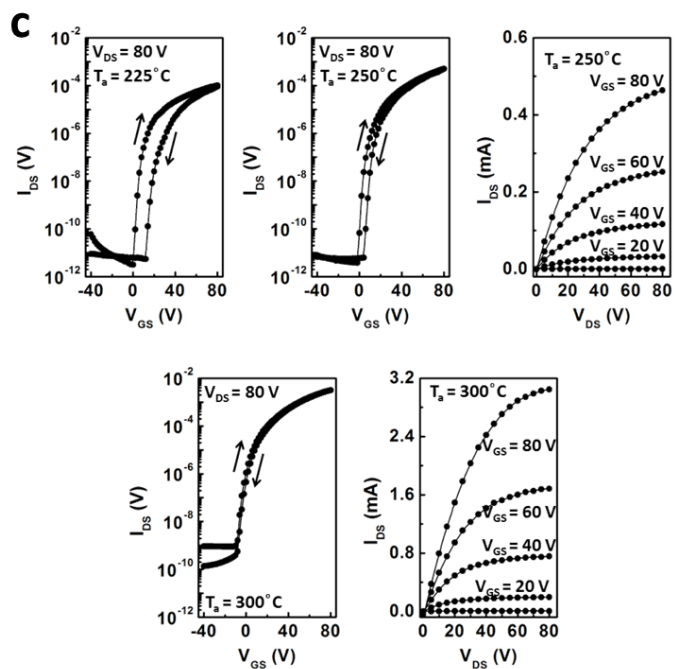
Figure S12. Transfer and output plots of the SCS 20 nm thick oxide films at various processing temperatures (on 300 nm SiO_2/Si substrates): **a,** In_2O_3 films, **b,** IZO films, **c,** IGZO films.
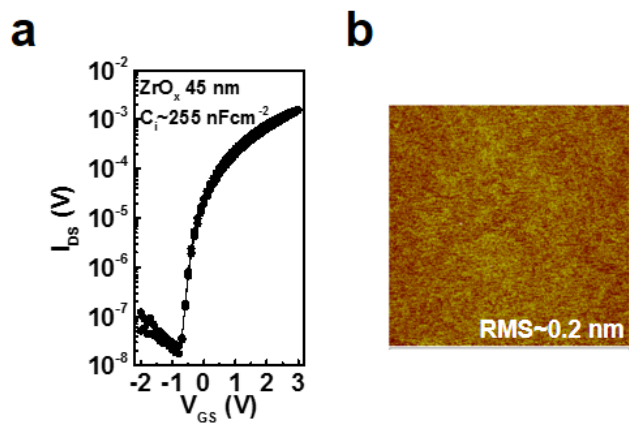
a

b

Figure S13. Representative transfer plot for a 20 nm thick SCS IZO film on 45 nm ZrO_2/ITO glass substrates processed at 300 °C. The FET mobility of this device is ~ 90 cm2Vs-1.

a

SCS IGZO

u_{lin} ~ 6.5 cm²/Vs
u_{sat} ~ 6.2 cm²/Vs

V_D = 5V
V_D = 80V

I_{DS} (A)

V_{GS} (V)

b

Sputter IGZO

u_{lin} ~ 11.4 cm²/Vs
u_{sat} ~ 10.8 cm²/Vs

V_D = 5V
V_D = 80V
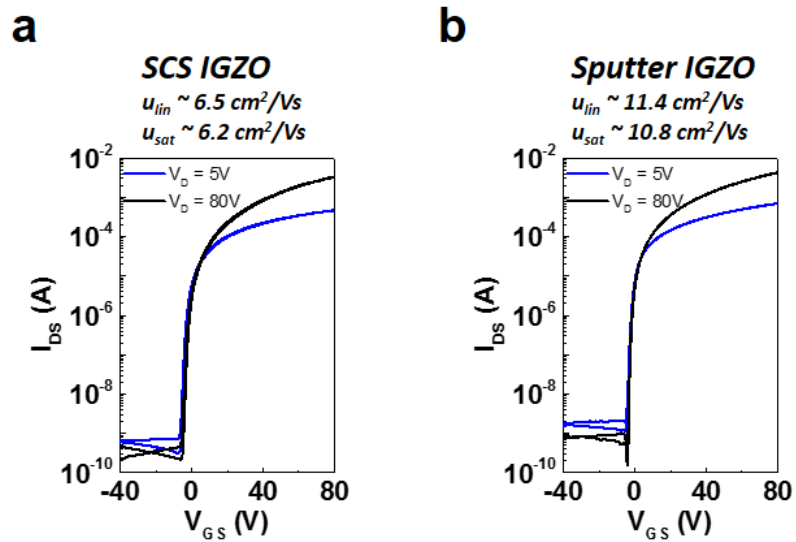
I_{DS} (A)

V_{GS} (V)

Figure S14. Representative transfer plots for SCS (20 nm, processing at 300 °C) and sputtered IGZO TFTs.
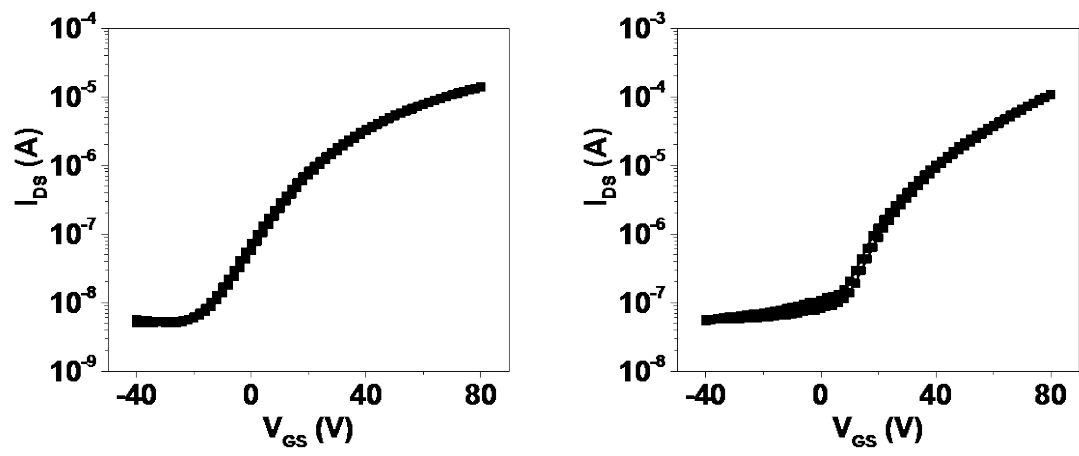
Figure S15. Representative transfer plots for two Spray IGZO TFTs without fuel processed at 300 °C.
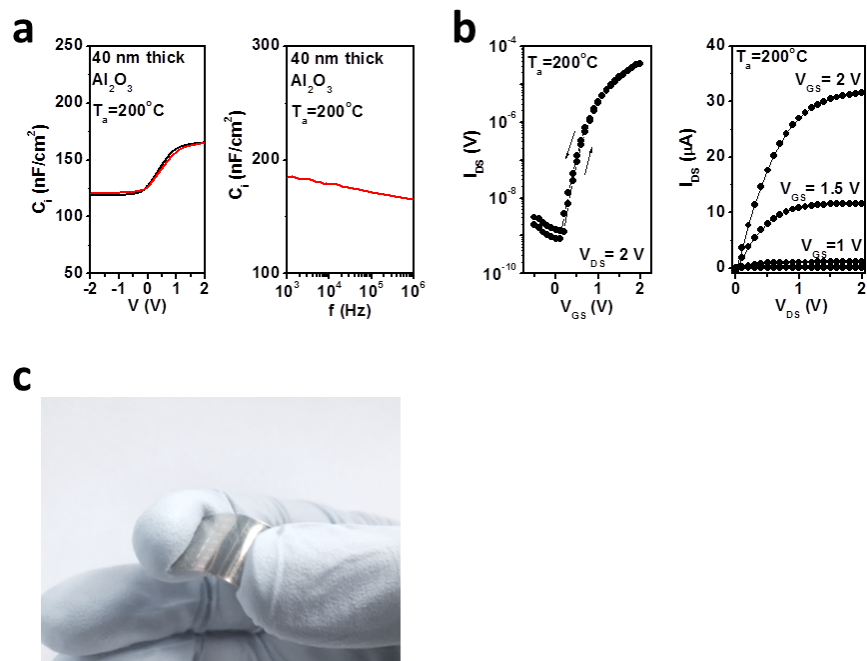
Figure S16. **a.** Characterization of 40 nm Al_2O_3 dielectric layers processed at 200 °C: C-V measurements at 10 kHz, and frequency measurements at 2 V. **b,** Transfer and output characteristics of the SCS flexible In_2O_3 films (on 40 nm Al_2O_3/Arylite substrates) processed at 200 °C. **c,** Optical image of flexible SCS In_2O_3 TFTs on an Arylite substrate (40 nm Al gate electrode/40 nm Al_2O_3 dielectric, with 40 nm Al source and drain electrodes).
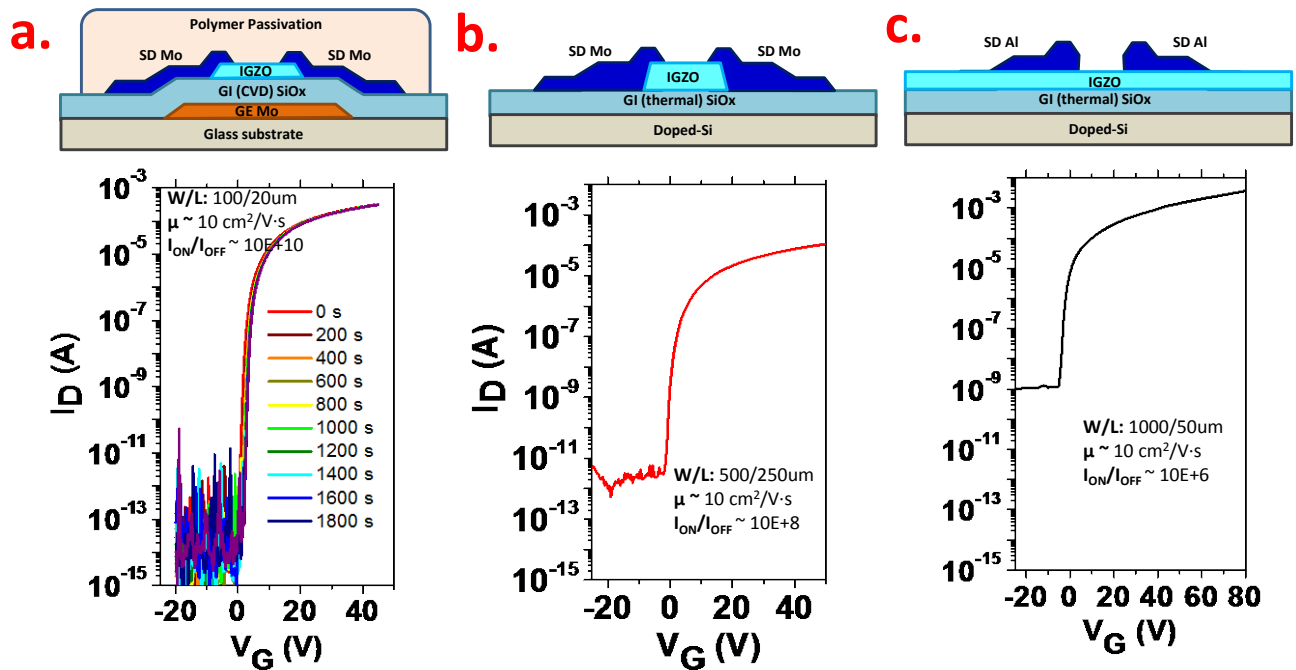
Figure S17. **a. Top.** Schematic representation for a fully patterned sputtered IGZO TFT. **Bottom.** Representative I-V plots (V_D = 45 V) corresponding to a negative bias stress experiment (V_D = 10 V, V_G = -30 V, T = 60°C, 5 min cycle). **b. Top.** Schematic representation for a sputtered IGZO TFT with patterned only the IGZO layer. **Bottom.** Representative I-V plot (V_D = 45 V). **c. Top.** Schematic representation for a sputtered IGZO TFT without patterning as used in this study. **Bottom.** Representative I-V plot (V_D = 80 V). GE = gate electrode, GI = gate insulator.
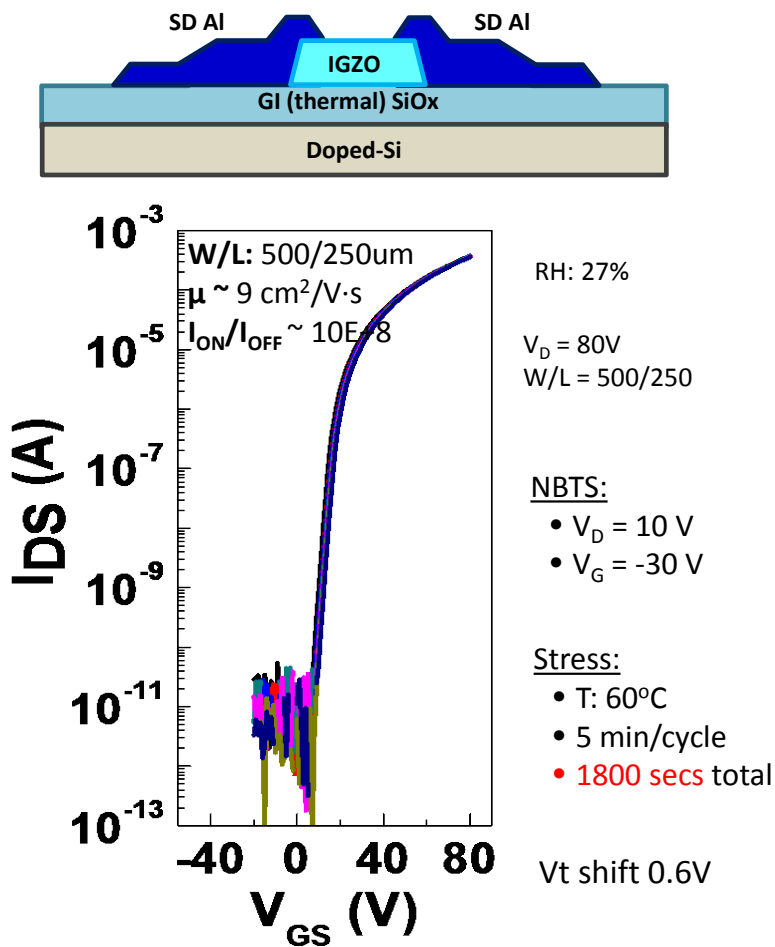
SD Al   **SD Al**

IGZO

GI (thermal) SiOx

Doped-Si

W/L: 500/250um
$\mu \sim 9\ cm^2/V\cdot s$
$I_{ON}/I_{OFF} \sim 10E/8$

RH: 27%

$V_D = 80V$
W/L = 500/250

NBTS:
• $V_D = 10\ V$
• $V_G = -30\ V$

Stress:
• T: 60°C
• 5 min/cycle
• 1800 secs total

Vt shift 0.6V

Figure S18. **a. Top.** Schematic representation for a fully patterned sputtered IGZO TFT. **Bottom.** Representative I-V plots ($V_D = 45$ V) corresponding to a negative bias stress experiment ($V_D = 10$ V, $V_G = -30$ V, T = 60°C, 5 min cycle). GI = gate insulator.
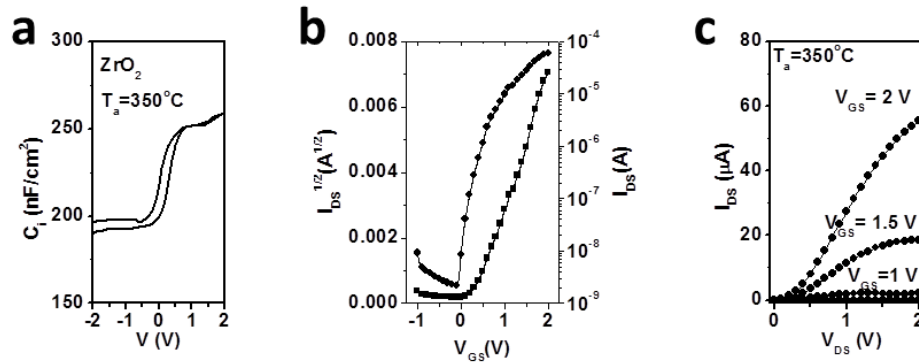
Figure S19. **a**. C-V measurements of 45 nm ZrO_2 dielectric layers processed at 350 °C at 10 kHz. **b**. Transfer and **c**. output characteristics of the SCS flexible IGZO111 (on 45 nm ZrO_2/ITO glass substrates) processed at 350 °C.
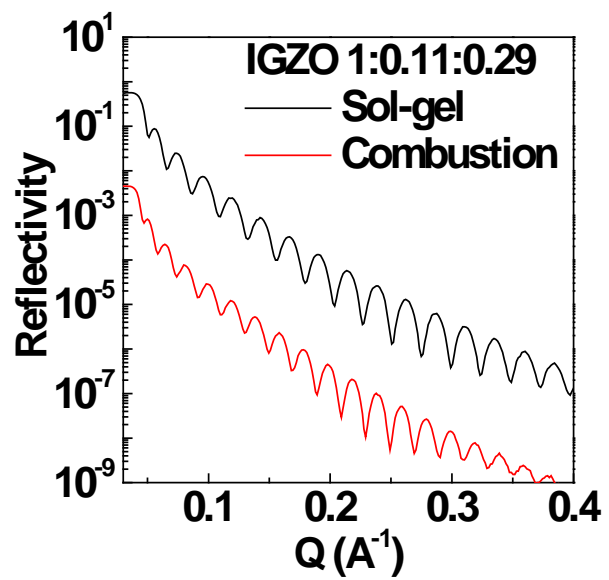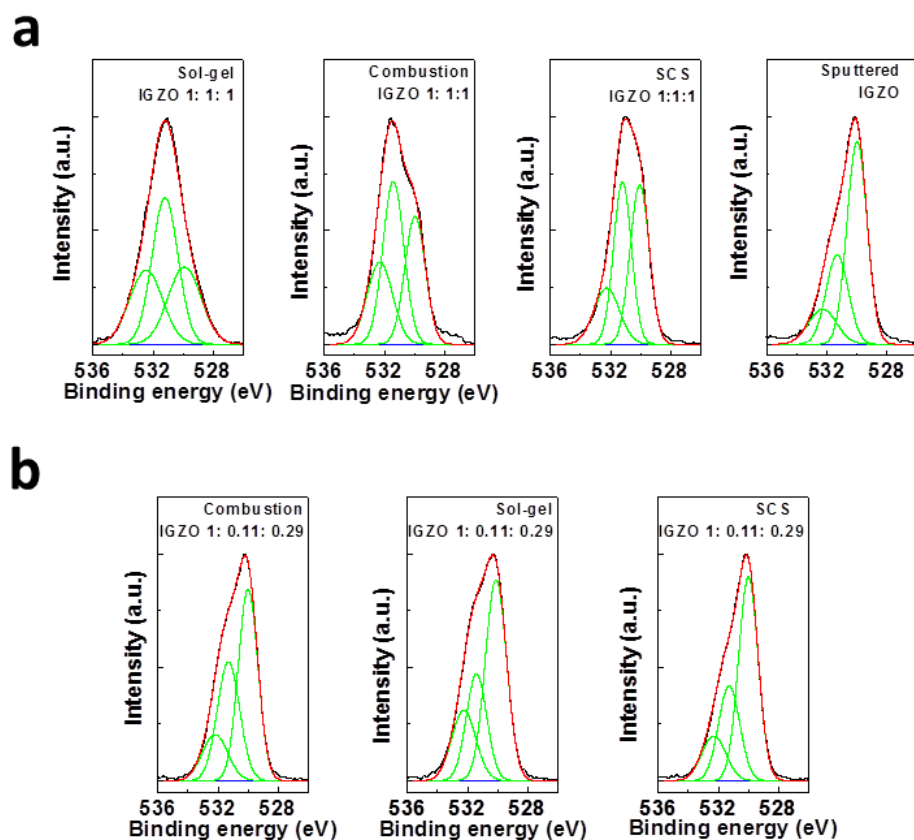
Figure S20. XRR of IGZO films with composition 1:0.11:0.29 by sol-gel and spin-SC

.

	IGZO 111			IGZO 1:0.11:0.29		
	M-O-M (%)	M-OH (%)	Other O (%)	M-O-M (%)	M-OH (%)	Other O (%)
Sol-gel	0.31	0.38	0.31	0.52	0.27	0.21
Spin-CS	0.32	0.42	0.26	0.49	0.35	0.16
SCS	0.45	0.41	0.14	0.56	0.29	0.15
Sputtering	0.58	0.28	0.14			

Figure S21. X-ray photoelectron spectra of 50 nm thick IGZO films by various deposition methods: **a,** with composition (In:Ga:Zn=111, solution processed IGZOs were annealed at 350 °C). **b,** with composition (In:Ga:Zn= 1: 0.11: 0.29, processed at 300 °C). The table summarizes the O% from deconvolution analysis
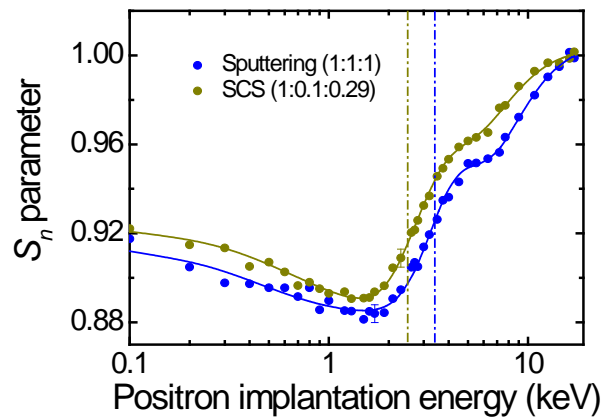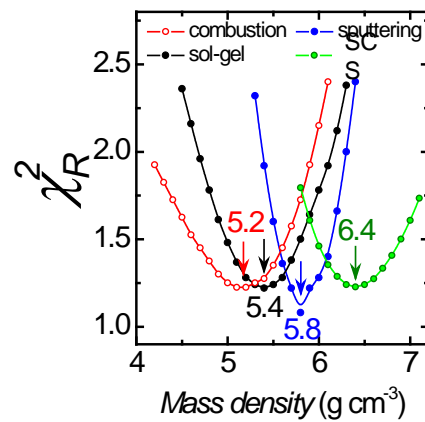
Figure S22. **a**, S_r parameter as a function of the positron implantation energy. The continuous lines are the best fits using three-layer model using VEPFIT. The vertical dashed lines mark the position of the nominal interfaces IGZO/SiO$_2$. Error bars are shown for one point only in each evolution. **b**, Reduced chi-square statistic of the S_r-parameter (calculated for thicknesses lower than 100 nm) as a function of the number density of the IGZO films.

a, Carrier density:
$$n = n_i e^{q\phi/KT}$$

$Q = CV$
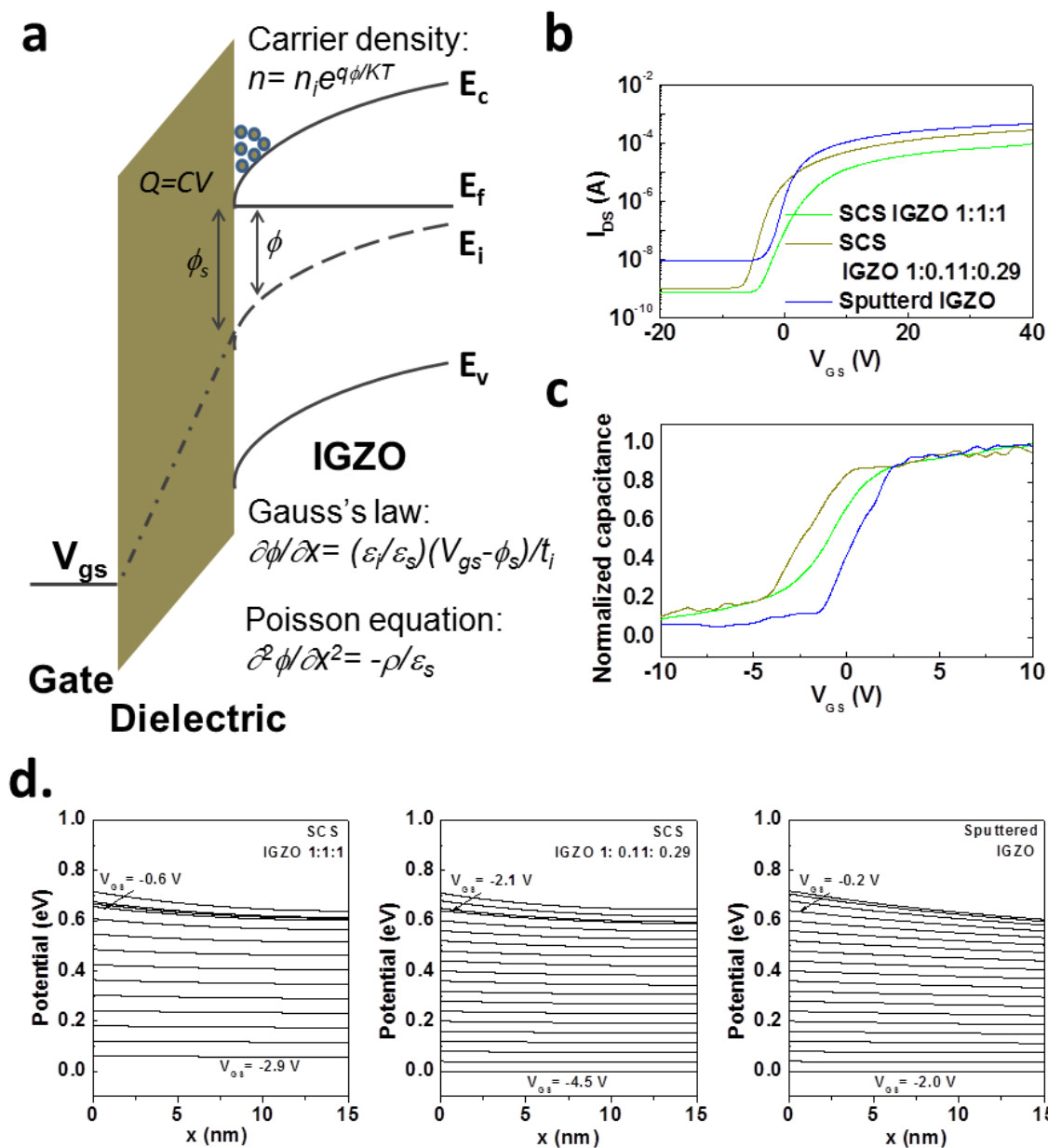
IGZO

Gauss's law:
$$\partial\phi/\partial x = (\varepsilon_i/\varepsilon_s)(V_{gs} - \phi_s)/t_i$$

Poisson equation:
$$\partial^2\phi/\partial x^2 = -\rho/\varepsilon_s$$

Gate Dielectric

b

SCS IGZO 1:1:1
SCS IGZO 1:0.11:0.29
Sputterd IGZO

c

d.

Figure S23. **a**, Energy band depth profile in IGZO TFT devices. **b**, Transfer I_{DS}- V_{GS} curves (at low V_{DS} 5 V) and **c**, capacitance voltage C-V characteristics of sputtered and two SCS IGZO (In:Ga:Zn=111 and 1: 0.11: 0.29) films deposited on ultra-low resistivity Si (ρ as small as 0.001)/CVD SiN$_x$(200 nm)/SiO$_x$ (100 nm) substrates. TFTs: Conventional sol-gel deposited; Combustion post annealing deposited; **d**, Spatial profiles of surface bend bending for the corresponding IGZO films.

Table S1. Results obtained in the IGZO/SiO$_2$/Si heterostructure from the positron lineshape profiles (Fig. 4c) using VEPFIT. Positron diffusion length L_+, thickness Z, S_r-parameter and F_{3y} fraction. The thickness, the positron diffusion length and the S_r-parameter of the SiO$_2$ film in all cases were: 300(8) nm, 16(2) nm and 0.981(2), respectively. The positron diffusion length in the p-Si substrate was 110(20) nm. Fixed parameters are denoted with the letter F.

	L_+ (nm)	Z (nm)	S_r-parameter	F_{3y} %
sputtered (1:1:1)	12(2)	55 F	0.878(1)	0.7(5)
sol-gel (1:1:1)	6(2)	32 F	0.933(1)	5.2(6)
spin-CS (1:1:1)	5(2)	27 F	0.932(1)	5.0(6)
SCS (1:1:1)	10(2)	50F	0.904(1)	2.1(5)
SCS (1:0.1:0.29)	11(2)	27 F	0.881(1)	0.9(5)

Table S2. Mass Densities of In$_2$O$_3$, Ga$_2$O$_3$, ZnO single crystal powders.

Metal Oxide	**Density (g cm^{-3})**	**Reference**
In$_2$O$_3$	7.18	9-11
Ga$_2$O$_3$	6.44	12,13
ZnO	5.61	14,15

Table S3. Conductivity and thickness of ITO films fabricated by the indicated methods.

	ITO films		
	Conventional sol-gel	Combustion spin	SCS
Conductivity (S cm^{-1})	81.2±12.9	127.4±10.1	174.6±12.5
Thickness (nm)	~105	~107	~96

References

[1] Pal, B. N., Dhar, B. M., See, K. C. & Katz, H. E. *Nat. Mater.* **8**, 898 (2009).

[2] Lee, C.-G. & Dodabalapur, A. *Appl. Phys. Lett.* **96**, 243501 (2010).

[3] Gidley, D. W., Peng, H. G. & Vallery, R. S. *Annu. Rev. Mater. Res.* **36** 49 (2006).

[4] Consolati, G. Ferragut, R. Galarneau, A. Renzo, F. D. & Quasso, F. *Chem. Soc. Rev.* **42**, 3821 (2013).

[5] van Veen, A., Schut, H., de Vries, J., Hakvoort, R. A. & Upma, M. R. AIP Conf. Proc. 218 Shultz, P. J., Massoumiand, G.R., Simpson, P. J., Ed.; *AIP: New York* 1990; pp 171-196.

[6] Tuomisto, F. & Makkonen, I. *Rev. Mod. Phys.* **85**, 1583-1631 (2013).

[7] Brusa, R. S., Karwasz, G. P., Mariotto, G., Zecca, A., Ferragut, R., Folegati, P., Dupasquier, A., Ottaviani, G. & Tonini, R. *J. Appl. Phys.* **94**, 7483-7492 (2003).

[8] Nomura, K., Kamiya, T., Ohta, H., Uruga, T., Hirano, M. & Hosono, H. *Phys. Rev. B* **75**, 035212 (2007).

[9] Dahlberg, S. C. *Surf. Sci*. **60**, 231 (1976).

[10] Bell, R. L. & Uebbing, J. J. *Appl. Phys. Lett.* **12**, 76 (1968).

[11] Hewitt, R. W. & Winograd, N. *J. Appl. Phys.* **51**, 2620 (1980).

[12] *CRC Handbook of Chemistry and Physics* I989-1990 p. B-92 (CRC, Boca Raton,1989).

[13] Passlack, M., Schubert, E. F., Hobson, W. S., Hong, M. N., Moriya, S., Chu, N. G., Konstadinidis, K., Mannaerts, J. P., Schnoes, M. L. & Zydzik, G. J. *J. Appl. Phys.* **77**, 686 (1995).

[14] Donnay, J. D. H. & Ondik, H. M. Inorg. Compounds, Publ. jointly by U.S. Dept. of Commerce, NBS and Joint Committee on Powder Diffraction Stds. (1973).

[15] Merrill, L. *J. Phys. Chem.* Reference Data **6**, 1205 (1977).